Construction and Building Materials 260 (2020) 119927

Contents lists available at ScienceDirect

Construction and Building Materials

journal homepage: www.elsevier.com/locate/conbuildmat

Molecular dynamics simulation of the interfacial bonding properties between graphene oxide and calcium silicate hydrate

Pan Wang [a], Gang Qiao [a], Yupeng Guo [b], Yue Zhang [a], Dongshuai Hou [a,*], Zuquan Jin [a], Jinrui Zhang [c], Muhan Wang [a], Xiaoxia Hu [a]

[a] Department of Civil Engineering, Qingdao University of Technology, Qingdao 266033, China
[b] College of Engineering, Huazhong Agricultural University, Wuhan 430070, China
[c] State Key Laboratory of Hydraulic Engineering Simulation and Safety, Tianjin University, Tianjin 300072, China

HIGHLIGHTS

- The impact of functional groups on the interfacial bonding strength of GO/C-S-H has been explored and explained.
- The local structure of GO/GN on the C-S-H substrate was depicted.
- Interfacial shear strength of GO/C-S-H composite is reduced with moisture content increasing.

ARTICLE INFO

Article history:
Received 10 March 2020
Received in revised form 7 June 2020
Accepted 10 June 2020
Available online 28 June 2020

Keywords:
Graphene oxide
Calcium silicate hydrate
Interfacial bonding properties
Molecular
Dynamics simulation

ABSTRACT

This paper investigates interfacial characteristics between graphene oxide (GO) and calcium silicate hydrate (C-S-H) composite using molecular dynamics simulations. Effects of functional group types (carboxyl and hydroxyl functional groups) and water content on the interfacial bonding strength were studied. Simulation results reveal that the interfacial bonding strength between GO and C-S-H is enhanced significantly than that of between pristine graphene sheet (GN) and C-S-H, which ascribes to the stability of chemical bond connection and mechanical interlocking. The interfacial bonding strength decreases with the decrease of water content, which indicates that invaded water could weaken the GO and C-S-H adhesion.

1. Introduction

Ordinary Portland cement, the key ingredient of concrete, is indispensable in civil engineering [1]. More than 3.6 billion tons of cement is produced per year to meet the needs of urbanization [2]. In particular, modern concrete structures for sea-crossing bridges, high-speed railways, nuclear power projects, and ultrahigh-rise buildings have put forward higher requirements of safety, durability, and functionality. Due to the quasi-brittle nature, ordinary concrete materials are poor to resist crack formation [3–5]. To overcome the above shortcomings, the reinforcing materials, such as steel fibers [6], polymer fibers [7–9], mineral fibers [10,11], have been used to control and reduce the crack formation in fiber reinforce concrete (FRC).

The improvement in mechanical properties of FRC ascribes to the replacement of the large cracks in concrete with the micro cracks [12], but those reinforce fibers fail to stop nanoscopic crack initiation. As, the emergence and development of nanotechnology, the addition of nanomaterials (nanosilica, carbon nanotube, and graphene, etc.) in cement materials have become a promising strategy to control the growth of nanoscale cracks in the cement materials, which further improves the mechanical performance of cement materials [13–15]. Among these nanomaterials, graphene and its derivatives have attracted great interest owing to their excellent physico-mechanical properties [16–19]. Pristine graphene possesses superb mechanical property (the Young' s modulus is ~ 1 TPa and the tensile strength is ~ 130 GPa [20–22]) and large aspect ratio (greater than3000 [23,24]), which makes it a good candidate as reinforce additive; but the poor dispersing property of pristine graphene in cement matrix restricts

* Correspondence author.
E-mail addresses: wangpan@qut.edu.cn (P. Wang), 1156860382@qq.com (G. Qiao), guoyp2016307@163.com (Y. Guo), zhangyue1723@gmail.com (Y. Zhang), dshou@outlook.com (D. Hou), jinzuquan@sohu.com (Z. Jin), jinrui.zhang@tju.edu.cn (J. Zhang), wangmuhan@qut.edu.cn (M. Wang), sasahuxiaoxia@163.com (X. Hu).

https://doi.org/10.1016/j.conbuildmat.2020.119927
0950-0618/

its applications [25,26]. Graphene oxide (GO) is an important kind of graphene derivatives with better dispersibility which has been widely applied in material modification, seawater purification, and many other industries [27,28]. Recently, the incorporation of GO as nano-reinforcement in cement-based composites have attracted particular interest, and the reinforced effect of GO on the mechanical properties of cement matrix could be better than those of graphene sheets. With adding 0.03 wt% of GO in cement matrix, the tensile strength of cement composite could be increased by ~40% [29]; the addition of 0.05 wt% GO could increase the compressive strength of cement composite by 15–33% and flexural strength by 41–59% [30].

Experimental results have demonstrated that GO reinforcement cement possesses excellent mechanical properties, but it challenges experimental technologies to clarify molecular mechanisms underlying the reinforcement. Molecular dynamics (MD) simulation provides a powerful computational tool in understanding the characteristics of the GO-cement composite, which can give fundamental insight into the microscopic reinforcement mechanism of GO-cement composite. As the key component to providing the binding strength within the cementitious materials, the calcium silicate hydrate (C-S-H) determines the mechanical performance and the durability of cement material. Based on MD simulations and the C-S-H model, the study of cement has deepened into the nanoscale level. The mechanical properties, the adsorption behavior, and the transport properties of C-S-H matrix or C-S-H gel pore have been studied by MD methods [31–36]. Evaluated by uniaxial tension simulation, the mechanical properties of C-S-H show anisotropic and heterogeneous. Along the perpendicular direction to interlayer, the C-S-H gel is connected via noncovalent bond, which has the weakest tensile strength [31]. Water and ions in the C-S-H gel pores exhibit different transport behavior [33]. Besides, the interfacial connection properties of GO/C-S-H composite were also investigated via MD simulations. It has been found that hydrogen-bond forms between the hydroxyl groups in GO provide and water molecules in the C-S-H [34,35]. In addition, the enhancement of Young's modulus and strength of C-S-H with the incorporation of GO can also be assessed using MD simulations, which demonstrates that the strong interfacial interaction and mechanical interlocking is responsible for the enhancement [37]. These simulation works provide fundamental insights into the connecting mechanism of GO reinforcement cement-based material.

With the rapid development of chemical synthesis technology, GO treated with various species and different amounts of oxygen-containing functional groups can be easily synthesized by various treated methods [38,39]. These studies motivate us to investigate the controlling effects of GO with various oxygen-containing functional groups on the nanoscale crack in the cement materials. To do this, the adhesion properties between GO sheet and C–S–H matrix were investigated via MD simulations, and three models including graphene sheet (GN), GO with carboxyl group (GOOH), and GO with hydroxyl group (GOH) were considered. The interfacial bonding strength was evaluated during the pull-out simulation process. The underlying mechanism was uncovered from the interfacial chemical bond and mechanical interlocking. Besides, the influence of water content on the interfacial bonding properties was finally investigated by simulating the pull-out process. This study not only provides valuable information on the interfacial strengthening mechanism but also enlightens the design strategies of GO/cement composites.

2. Computational methods

2.1. Model

In this work, the GO/C-S-H composite models are used for investigating the interfacial bonding properties. The composite model contains two parts: C-S-H substrate, GN or GO sheets. The C-S-H substrate is built using the Tobermorite 11 Å, as shown in Fig. 1a, which has same chemical component and similar layered crystal structure with the C-S-H [40,41]. By expanding the unit cell of the Tobermorite 11 Å along the [001] direction, the C-S-H substrate with the crystal parameters a = 43.2 Å, b = 45.04 Å, c = 46.26 Å, $\alpha = \beta = \gamma = 90^0$ is obtained. Subsequently, one layer of bridged silicate tetrahedron in the center of crystal along Z direction is deleted. Non-bridging oxygen atoms are exposed in the C-S-H interface due to the deletion. A part of nonbridging oxygen atoms in the new cleaving surface of C-S-H substrate is protonated and

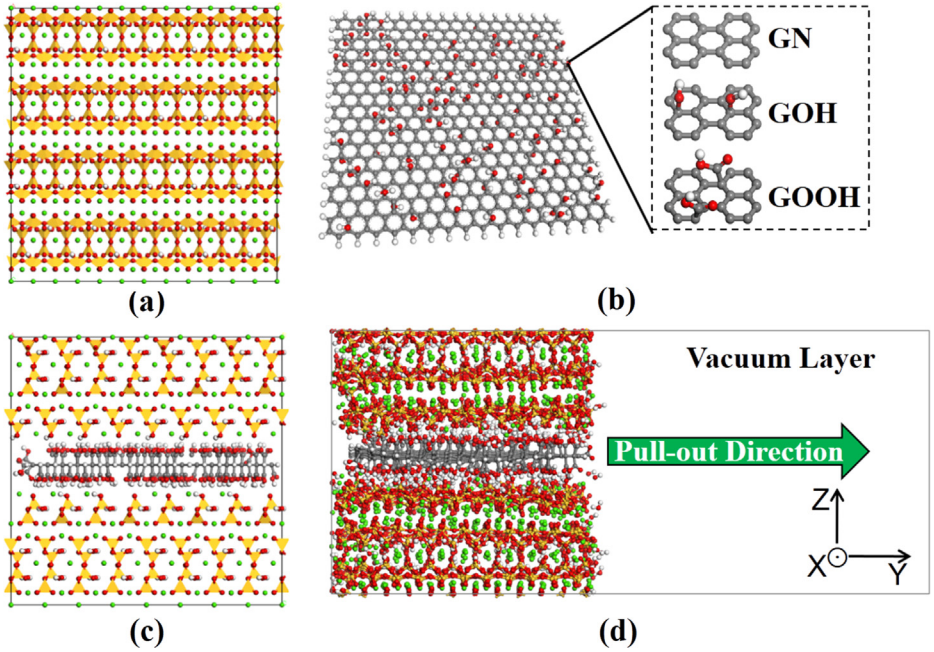

Fig. 1. (a) the cleaved tobermorite 11 Å model, (b) the GO sheet and functional groups, (c) the composite initial models, (d) the pull-out model.

some of Ca^{2+} atoms are deleted to maintain the charge balance of simulation system. The C-S-H substrate with a channel with the width of about 5 Å is produced.

The GN/GO sheets are constructed according to the modeling process by Allington et al. [42]. The lattice parameters pristine GN sheet unit cell is a = 3.69 Å, b = 4.62 Å, c = 3.4 Å, $\alpha = \beta = \gamma = 90^0$. The unit cell is expanded 11 times in the a-direction and 10 times in the b-direction to match the size of C-S-H substrate. Then, two different functional groups –COOH and –OH are bonded to the graphene surface. It has been reported experimentally that the typical surface coverage ratios of GO, the ratio of functional group and carbon atoms in GO, is about 20% [43]. The same ratio is adopted in our GO model. The pristine GN model is also studied for comparative analysis. The model of GN and GO are shown in Fig. 1b.

Afterward, the GN/GO sheets are planted in the cleaved region of C-S-H matrix to construct an initial model, as shown in Fig. 1c. Then, the pull-out model is constructed by adding the vacuum layer with thickness equal to 60 Å along y-direction, as shown in Fig. 1d.

2.2. Computational details

2.2.1. Force field

The atoms interaction of C-S-H is described by the Clayff force field [44], which has been successfully and widely applied to simulate the molecular structure and mechanical properties of C-S-H. The atom interaction of GN/GO is based on the consistent valence force field (CVFF) [45]. The simple point-charge (SPC) water model [46] is utilized for describing water molecules confined in the C-S-H gel. The mix arithmetic rule [47] is selected for the combination of different force fields. This combination force field has accurately and successfully simulated the properties of GO/C-S-H composites [48–50].

2.2.2. Molecular dynamic procedure

All simulation processes are implemented using the large-scale atomic/molecular massively parallel simulator (LAMMPS) platform [51]. The simulation process for the initial model (Fig. 1c) goes through two stages: the energy minimized and the pre-equilibrium process. During the energy minimized, all the atoms are relaxed. In the pre-equilibrium process, the simulations are conducted under NPT ensemble at 300 K and 1 atm for 2000 ps. The Nosé–Hoover approach is selected for the temperature and pressure control. During the simulation, the leapfrog algorithm is employed to integrate the equation of motion, and the time step was set to 1 fs. And trajectories of atoms data in the last 1000 ps are collected for analyzing the structure and dynamics properties of the composite interface.

2.2.3. Pull-out simulation

For pull-model (Fig. 1d), a pre-equilibrium process is performed under NVT ensemble for 2000 ps. The pull-out simulation under NVT ensemble is performed to obtain the load–displacement curves for characterizing the interfacial bonding properties. In the pull-out process, a row of carbon atoms on the right side of GN or GO is selected as the position for exerting external force, as shown in Fig. 1d. The external force value is shown as follow:

$$F = K((x_0 + v \times t) - x_{com}) \quad (1)$$

where F represents the external force; K represents the spring constant, which is set to 0.01 kcal/mol/nm^2; x0 is the initial center of mass (COM) of selected carbon atoms along the y-direction; v represents the pulling speed of the reference point along the y-axis and is 0.0025 nm/ps; t is the simulation time; x_{com} is the dynamics position along y-direction of COM of selected carbon atoms. The total simulation time of pull-out process is set to 2000 ps. The external force and x_{com} are collected to obtain the load–displacement curves.

3. Results and discussions

In this section, the adhesion properties of GO/C-S-H composite is investigated, and the load–displacement curve and the interfacial shear strength of the GO/GN-C-S-H composite are calculated, and the underlying mechanism is uncovered from interfacial chemical bond and mechanical interlocking. The effect of water content on the interfacial bonding properties was also elucidated.

3.1. Pull-out process and interfacial bonding properties

The dynamic pull-out process can give a straightforward picture of shape-structure change of GO/C-S-H composite. The pull-out process of GOOH from C-S-H is shown in Fig. 2, where a, b, c, d, and e represent simulation snapshots at 0 ps, 200 ps, 250 ps, 1000 ps, and 1600 ps, respectively. Simulation results show that some discontinuous wrinkles or corrugations appear as GOOH sheet gradually pulled out from the C-S-H substrate. To quantitatively exhibit the pull-out process, the time evolution of the external force and the COM of selected carbon atoms along y-direction were recorded, as shown in Fig. 2. Overall, the COM position shows a linear increasing trend against the simulation time, indicating that the GOOH sheet can be pulled out stably under the external force. However, the pull-out force has a larger fluctuation. The pull-out force can be considered as feedback of the interaction between C-S-H matrix and GOOH sheet, which has a direct relationship with the interfacial stress transfer. Therefore, the pull out force can be used to characterize the interfacial bonding properties. The fluctuation pull-out force denotes that the interfacial bonding properties have a larger fluctuation as the GOOH sheet pulled out from the C-S-H matrix.

Here, the force–displacement is also derived according to the COM-time and force–time curve, as shown in Fig. 3a. Owing to the stable chemical bonds formed between GO and matrix, the pull-out load of GO is relatively high during the pull-out process, whereas GN sheet has only VDW interaction with C-S-H which shows the weakest pull-out behavior. The maximum pull force (F_{max}) for GOOH, GO and GN are 9.98 × 10^{-9}N, 7.16 × 10^{-9}N, and 4.30 × 10^{-9}N, respectively. The interface shear strength is derived based on the load–displacement curves and is defined as:

$$\tau = \frac{F_{max}}{2ab}$$

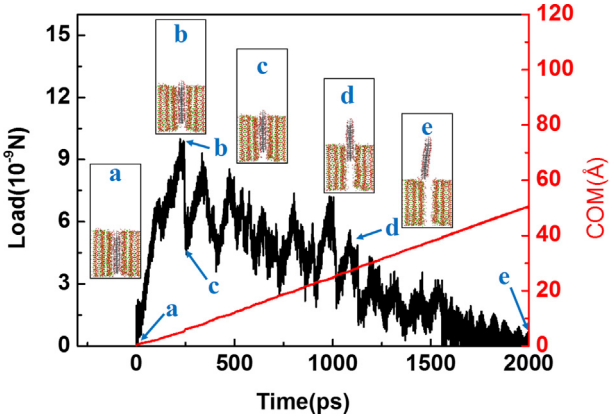

Fig. 2. Snapshot of pull-out process at 0 ps (a), at 1000 ps (b), and at 1600 ps (c), respectively. (d) The evolution of COM and the load.

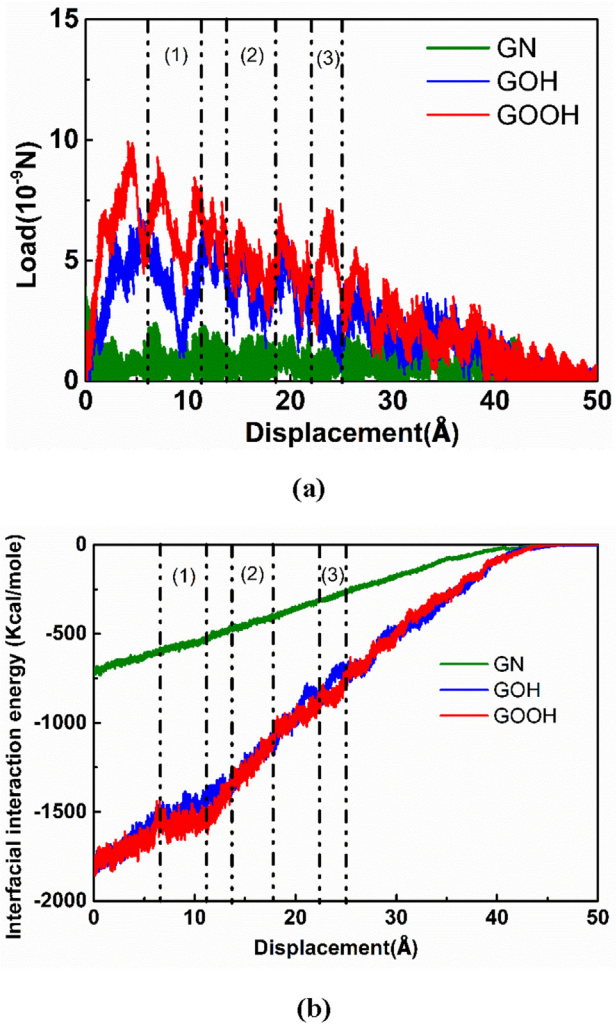

Fig. 3. (a) Load-Displacement curves for GN, GOH and GOOH, (b) Interfacial interactional energy of GN, GOH and GOOH.

where *a* and *b* are the width and length of GN or GO sheets. The interface shear strength of GO-COOH/C-S-H, GO-OH/C-S-H, and GN/C-S-H is 532 MPa, 383 MPa, and 230 MPa, respectively. The strong and stable chemical bonds formed at the GOOH/C-S-H and GOH/C-S-H surface bring on better pull-out behavior. Besides, as presented in Fig. 3b, the change of interfacial interaction energy between C-S-H and GO sheets in the pull-out process also shows higher than that of GN. It can be concluded that the higher interfacial bonding properties in GO-COOH/C-S-H composites are achieved compared to that of GO-OH/C-S-H composites followed by GN/C-S-H composite. This is consistent with a previous experimental study reported by Geng [52], in which they found the bonding strength between the carboxylic carbon nanotubes and cement matrix is higher than that of pristine carbon nanotubes. Thus, the GOOH or the GOH sheet can interact with the C-S-H gel more effectively than the pristine GN, and control concrete cementations material nanocrack better.

Besides, it can be seen in Fig. 3a that the force–displacement curve of GOOH and GOH models shows many peaks during the pull-out process, which is a typical "stick–slip" phenomenon. A similar phenomenon was also observed in previous studies [53]. The "stick–slip" phenomenon can be attributed to the repeated process of breaking-reconnection of bonds between GO and C-S-H. Taking the GOOH as an example, in the stick stage, the force increased rapidly in the first 5 Å displacements, it reaches its highest value, about 18×10^{-10}N. In the slip stage, the force abruptly drops to 10×10^{-10}N within 1 Å displacement. As mentioned above, the pull-out force during the pull-out process can be affected by two mechanisms: the pull-out force could be influenced by mechanical interlocking caused by surface roughness of the GO/GN; it could also be affected by interfacial chemical bonds between GO and C-S-H substrate. The discrepancy of interfacial shear strength for different GO/GN sheets was discussed from these two aspects.

3.2. Interfacial chemical bonds

To reveal the effect of interfacial interaction, the local structure of GO/GN on the C-S-H substrate was evaluated. Firstly, local atom intensity of GO/GN was calculated for the equilibrated composite system. Fig. 4 shows the variation of local atom intensity along the direction perpendicular to the C-S-H surface. The local atom intensity of Ca in the C-S-H matrix was also calculated for comparison analysis. The bottom of the model (Fig. 1d) is the origin of Z direction (Z = 0 Å) and the location of the interfacial oxygen atom in hydroxyl group is defined as the interface displayed by the gray line. As shown in Fig. 4, The channel width of the C-S-H substrate is increased greatly with the insertion of GO, attributed to the functional group in the GO sheet that could occupy the space. Moreover, the local atom intensity of Ca atoms shows a different distributed manner. In Fig. 4a, almost all the Ca atoms are presented on C-S-H side for GN/C-S-H composite system, while the intensity curve shifts to the GO side for GO/C-S-H composite system, indicating GO has much stronger interfacial interaction to C-S-H matrix than the pristine GN sheet. Comparing with the GN/C-S-H composite model, the peak value of the C atom of GO/C-S-H composite model is distributed widely, indicating that the added functional group can improve the interfacial interactions. This strong interaction makes the GO sheet failed to keep flaky shape anymore, causing increased surface roughness. The surface roughness mechanical interlocking will be further discussed in the 3.3 section.

To investigate the local chemical environments and interfacial interaction between GO and C-S-H substrate, the radial distribution functional (RDF) and coordination number (CN) were calculated. To distinguish the oxygen type in different positions, different kinds of oxygen atoms were defined. In particular, O_{nb} is the non-bridge oxygen atoms in a silicon tetrahedron in C-S-H, O_{oh} represents the hydroxyl oxygen atoms in C-S-H, O_{GOH} is the oxygen atom that in the GOH sheet, O_{GOOH} denotes the oxygen atom that in the GOOH sheet. Besides, O_{GOOH} is divided into two types according to their positions: O_1 denotes the oxygen atom that connects the carbon with double bonds, O_2 represents the oxygen atom that connects the carbon with a single bond. H_{oh} represents the hydroxyl hydrogen atoms in C-S-H. As shown in Fig. 5a, the RDF curves of O_{GOH}-Ca, O_{nb}-Ca, O_{oh}-Ca show a sharp peak located at about 2.35 Å, which represents these oxygen atoms can all form ionic bonds with Ca. These bonds connection can be observed in Fig. 6a, where the Ca atoms act as a bridge between GOH sheet and C-S-H substrate by O_{GOH}-Ca connection and O_{nb}-Ca or O_{oh}-Ca connection. In addition, the RDF curves of H_{oh}-O_{GOH} also have a broadening peak located at about 2 Å. It indicates the H bonds connection can be formed between GOH sheet and matrix, as shown in Fig. 6b. Comparing with the GOH/C-S-H composite system, the position of the RDF curve peaks for O-Ca connection in GOOH/C-S-H composite system (Fig. 5b) remains unchanged, whereas the peak gets sharper. It means the same

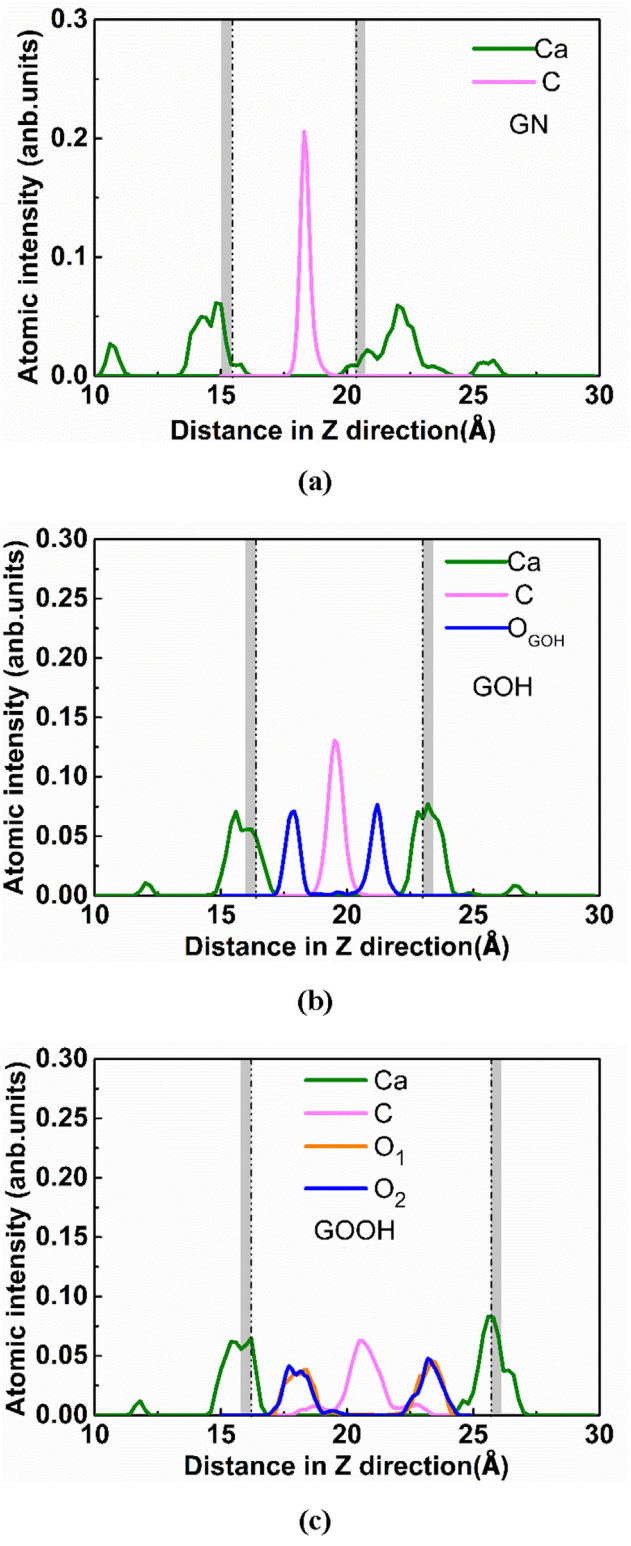

Fig. 4. Atomic intensity profiles along the Z direction.

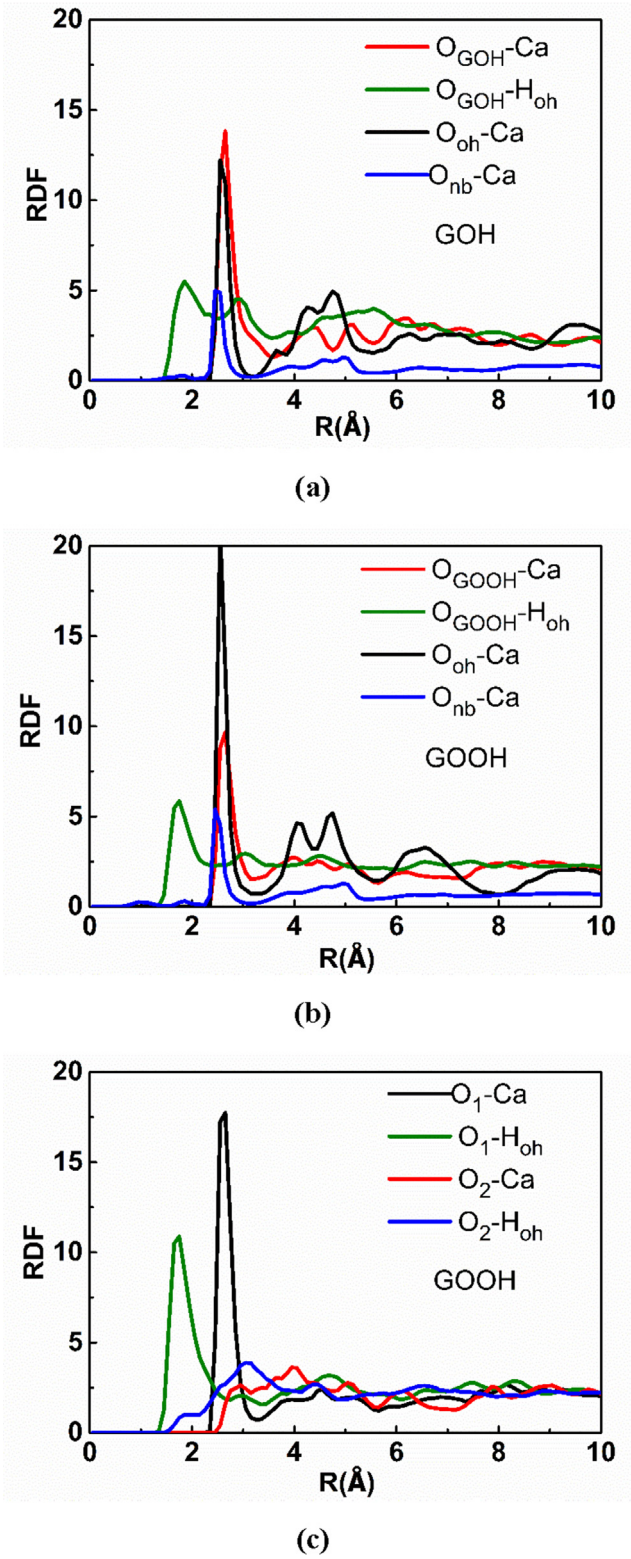

Fig. 5. Radial distribution function.

interfacial connection for GOH and GOOH, but the GOOH has stronger interfacial bonding interaction. The interfacial bonding connection between GOOH sheet and C-S-H substrate is also provided in Fig. 6cd. Moreover, to quantitatively characterize these two types of oxygen atoms in GOOH sheet, the RDF of O_1-Ca, O_2-Ca, O_1-H_{oh}, and O_1-H_{oh} were also plotted in Fig. 5d. The RDF of O_1-Ca and O_1-H_{oh} have an obvious peak, while the peak of O_2-Ca and O_2-H_{oh} are not obvious. It represents that the contribution of double bonds oxygen atoms to the interfacial strength is more than that of single bond oxygen atoms.

The coordinate number (CN) of Ca atoms and H_{oh} atoms is obtained by integrating the first peaks of RDF to make a detailed

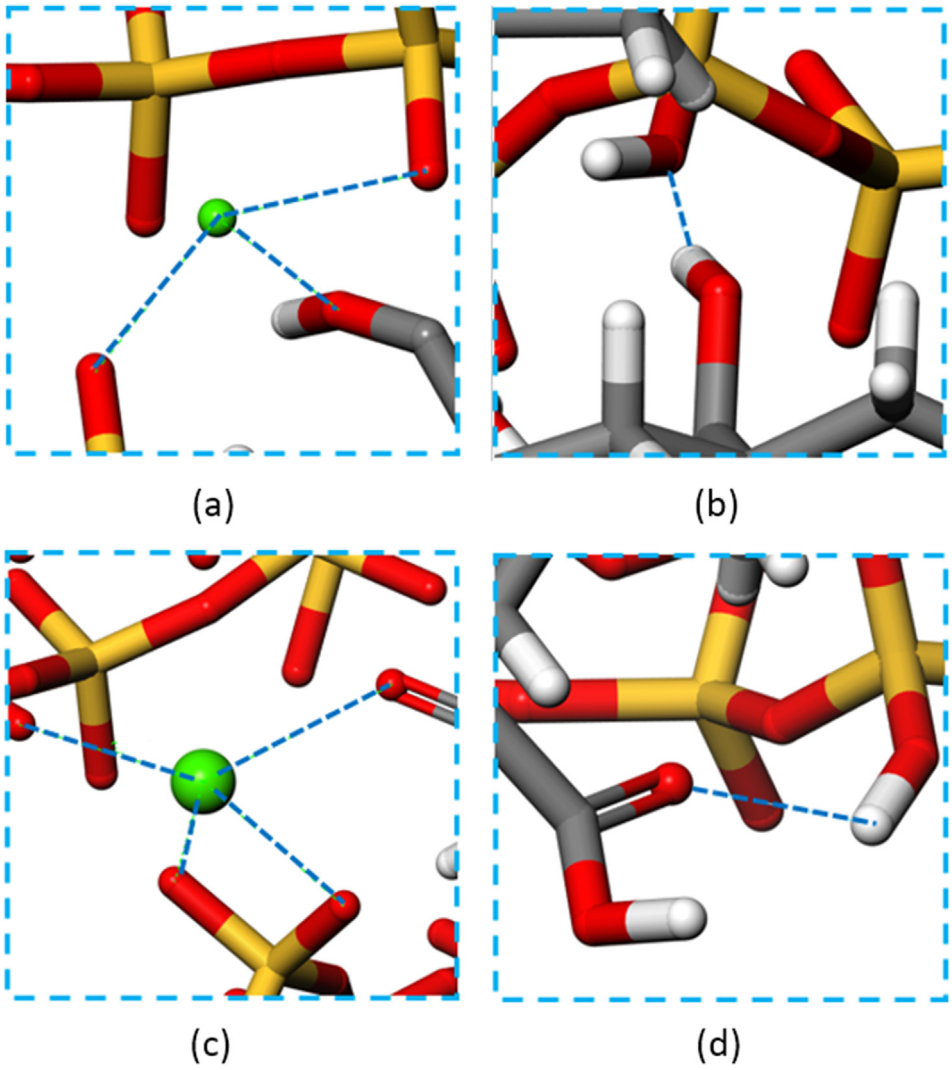

Fig. 6. Snapshots of chemical bonds.

Table 1
Coordinate number in GO-OH/C-S-H.

CN	Cut-off radius (Å)	Coordination number
Ca-O_{poly}	3.45	0.82
H_{oh}-O_{poly}	2.55	0.34
Ca-O_{oh}	3.15	0.16
Ca-O_b	3.45	4.22

Table 2
Coordinate number in GO-COOH/C-S-H.

CN	Cut-off radius (Å)	Coordination number
Ca-O_{poly}	3.45	1.17
H_{oh}-O_{poly}	2.55	0.53
Ca-O_{oh}	3.15	0.21
Ca-O_b	3.45	3.96
Ca-O_1	3.45	0.82
Ca-O_2	3.45	0.35
Hoh-O_1	2.55	0.42
Hoh-O_2	2.55	0.11

characterization of the ionic bonds, as presented in Table 1 and Table 2. For GOH/C-S-H composite system, the averaged CN of Ca-O_{GOH}, Ca-O_{nb}, and Ca-O_{OH} is about 0.82, 3.96, and 0.16, respectively. While for GOOH/C-S-H composite system, the averaged CN of Ca-O_{GOOH}, Ca-O_{nb}, and Ca-O_{OH} increases to 1.17, 4.12, and 0.21, respectively. As compared with the H_{oh}-O_{GOH}, the CN of H_{oh}-O_{GOOH} increases to 0.53. This indicates that the GOOH/C-S-H composite has more coordination connection than GOH/C-S-H composite. It is also found that the CN for O_1 around Ca or H_{oh} is higher than O2. This again reflects the interfacial strength of GOOH/C-S-H composites stems mainly from double bonds oxygen atoms.

As mentioned above, the interfacial bonding connection is demonstrated via RDF curve and CN. The stability of these bonding connections is reflected by the time correlation function (TCF). According to the definition of TCF [54], if the value of TCF remains at 1 during the whole simulation process, it indicates that the bond connection is very stable; By contrast, if the value of TCF degrades to 0, it suggests that the bonds connection is frequently broken and the chemical bond is unstable. Fig. 7a, Fig. 7b, and Fig. 7c show the TCF curves of Ca-O bonds. As shown in Fig. 7a, the TCF of Ca-O1 in the GOOH/C-S-H interface is always larger than that of Ca-O_{GOH} in the GOH/C-S-H interface. This indicates that the connection of Ca-O bonds in GOOH/C-S-H system is more stable. The TCF of Ca-O_2 degrades faster than that of Ca-O_1, which means the Ca-O_2 bonds are very weak. Fig. 7b exhibits the TCF for another chemical bond connection between GO sheet and C-S-H, which characterizes the

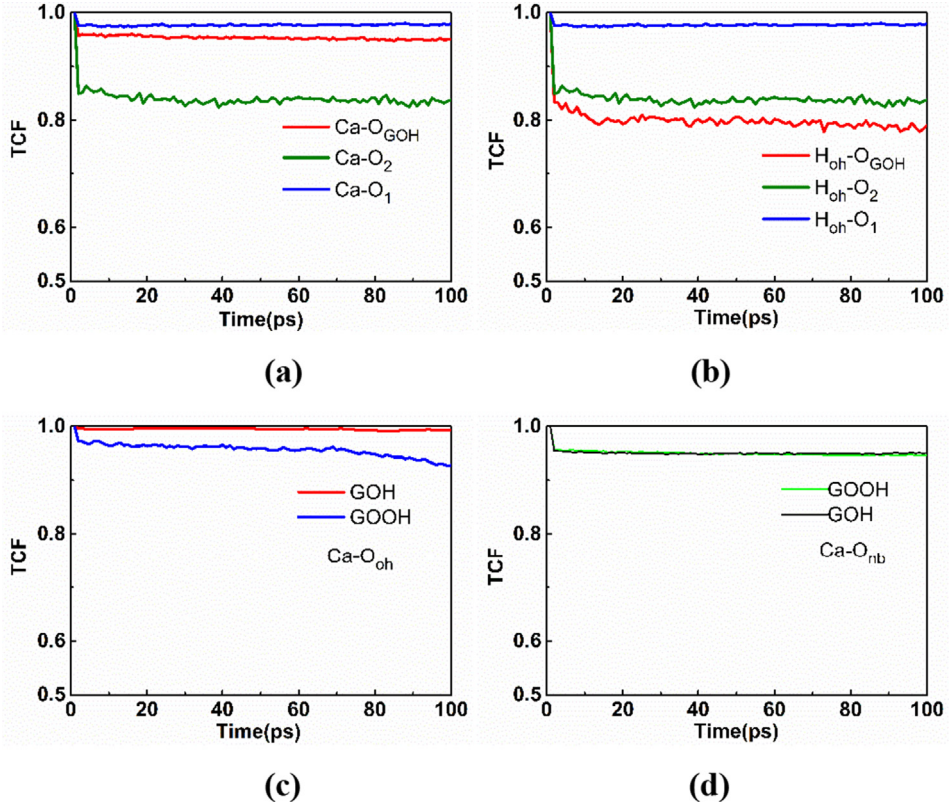

Fig. 7. Time-correlated function curve of Ca-O bond and H-O bond connection.

stability of H-O pairs. The TCF of O_{GOH}-H in GOH/C-S-H degrades faster than that of O_{GOOH}-H in GOOH/C-S-H systems, implying that the stable chemical bonds formed for GOOH/C-S-H systems. Fig. 7c and Fig. 7d show the TCF curve for Ca-O_{oh} and Ca-O_{nb}, which decreases slightly in the earliest stages and then remains at a high value. It indicates that the chemical bonds of Ca-O_{oh} and Ca-O_{nb} can last a long period.

3.3. Mechanical interlocking effect

The pull-out force is not only influenced by interfacial chemical bonds between GO and C-S-H substrate, but also influenced by mechanical interlocking caused by surface roughness of the GO/GN. Qualitatively, the interface configuration of GN, GOH, and GOOH in the channel region of the C-S-H was extracted, as shown in Fig. 8a, Fig. 8c, and Fig. 8e. It can be found that there are some discontinuous wrinkles or corrugations in the surface GN/GO sheets. Previous research also has confirmed the existence of corrugations in GN sheet [55]. The corrugations can be attributed to the change of the bond length of the C–C bonds in the GN sheet. The functional group in the GN sheet disturbed the bonding connection in the GN sheets, which will further affect the pull-out force via the mechanical interlocking effect resulted from surface roughness. More quantitatively, the z-position evolution of carbon atoms in GN or GO sheet was tracked to characteristic the surface roughness. As shown in Fig. 8b, d, and f, the maximum overlap degree of carbon atoms through observing the colors in the center and the distribution width of carbon atoms shows that the corrugations degrees of three sheets follow: GOOH > GOH > GN, which is consistent with the order of pull-out force.

3.4. Water content effect

It has been reported that the environmental humidity could significantly affect the structure and mechanical property of GO. As important constituent materials of infrastructure, the cement-based materials often suffer external water attacks. Owing to the hydrophilic nature of GO and C-S-H surface, the invasion water can be easily immobilized on the interlayer void between GO and C-S-H substrate. Thereby further affecting the performance of the interfacial interaction. In order to clarify the influence of humidity on the interfacial bonding strength between GO and C-S-H, three systems with different water content were constructed, including dry condition, one layer water molecules and two layer water molecules present on the interlayer void, as shown in Fig. 9a, Fig. 9b and Fig. 9c. The simulated method is the same as the case of dry model. The pull-out force–displacement curves of different water content for GN and GO are shown in Fig. 9 d, Fig. 9e and Fig. 9f. It can be seen that the pull-out force is significantly reduced with increasing water content.

The main reason is that the addition of water prevents the formation of chemical bonds between Ca ions and oxygen atoms in the silicon oxygen tetrahedron in C-S-H or oxygen atoms GO functional groups. As the water content increases, the interfacial chemical bonds are gradually replaced by a series of weakened hydrogen bonds, and water acts as a lubricant that weakens the interfacial bonding strength. The lubrication effect by surface layers of water has also been found in mica sheets channels [56]. Our simulation results reveal that in dry condition, there is close contact between GO sheet and C-S-H substrate, ensuring the strong interfacial bonding strength. However, in wet environment, the invasion of water molecules in the interlayer void between GO and C-S-H substrate could deteriorate the interfacial mechanical properties.

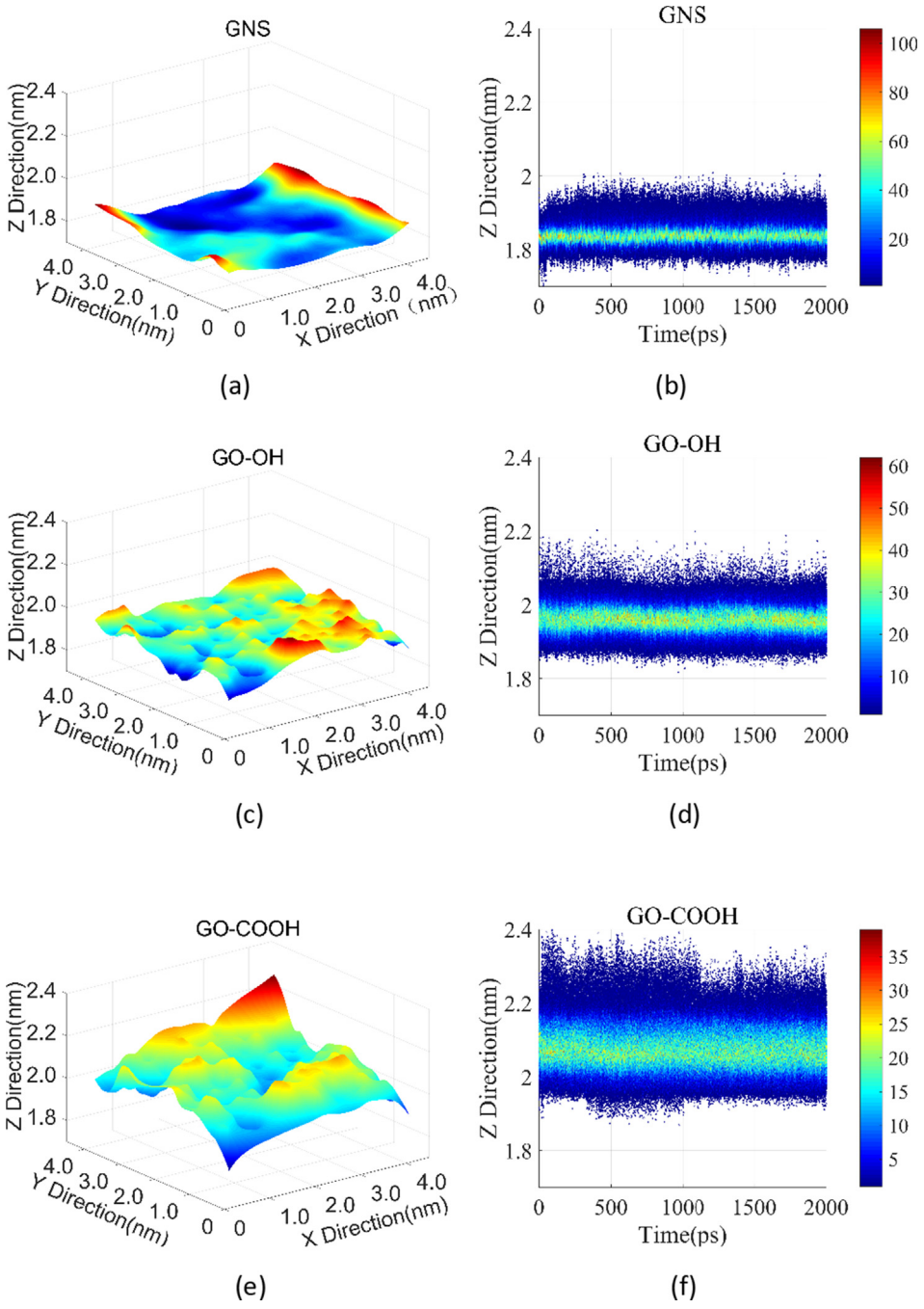

Fig. 8. The interface configuration of GN (a), GOH (c) and GOOH (e) in the channel region of the C-S-H substrate; The z-position evolution of carbon atoms in GN (b), GOH (d) and GOOH (f) sheet.

4. Conclusion

In this study, we investigated the structure, dynamics, and interfacial bonding properties of GO/C-S-H composites using MD simulations. Higher interfacial bonding properties in GOOH/C-S-H composites are achieved compared to that of GOH/C-S-H composites followed by GN/C-S-H composite. The ionic bonds and H bonds formed between GO and C-S-H, the mechanical interlocking caused by surface roughness of GO, both effects provide a contribution in enhancing the interfacial bonding strength. Compared to GOH/C-S-H composites, GOOH/C-S-H composites have better interfacial bond strength attributed to two important aspects: more and stable chemical bonds exist at GOOH/C-S-H composite interface; GOOH sheets show a higher level of surface roughness. In dry condition, there is close contact between GO and C-S-H, ensuring the strong interfacial bonding connection. However, in wet environment, the invaded water molecules in the interlayer void between GN/GO and C-S-H substrate weaken the GN/GO and C-S-H adhesion.

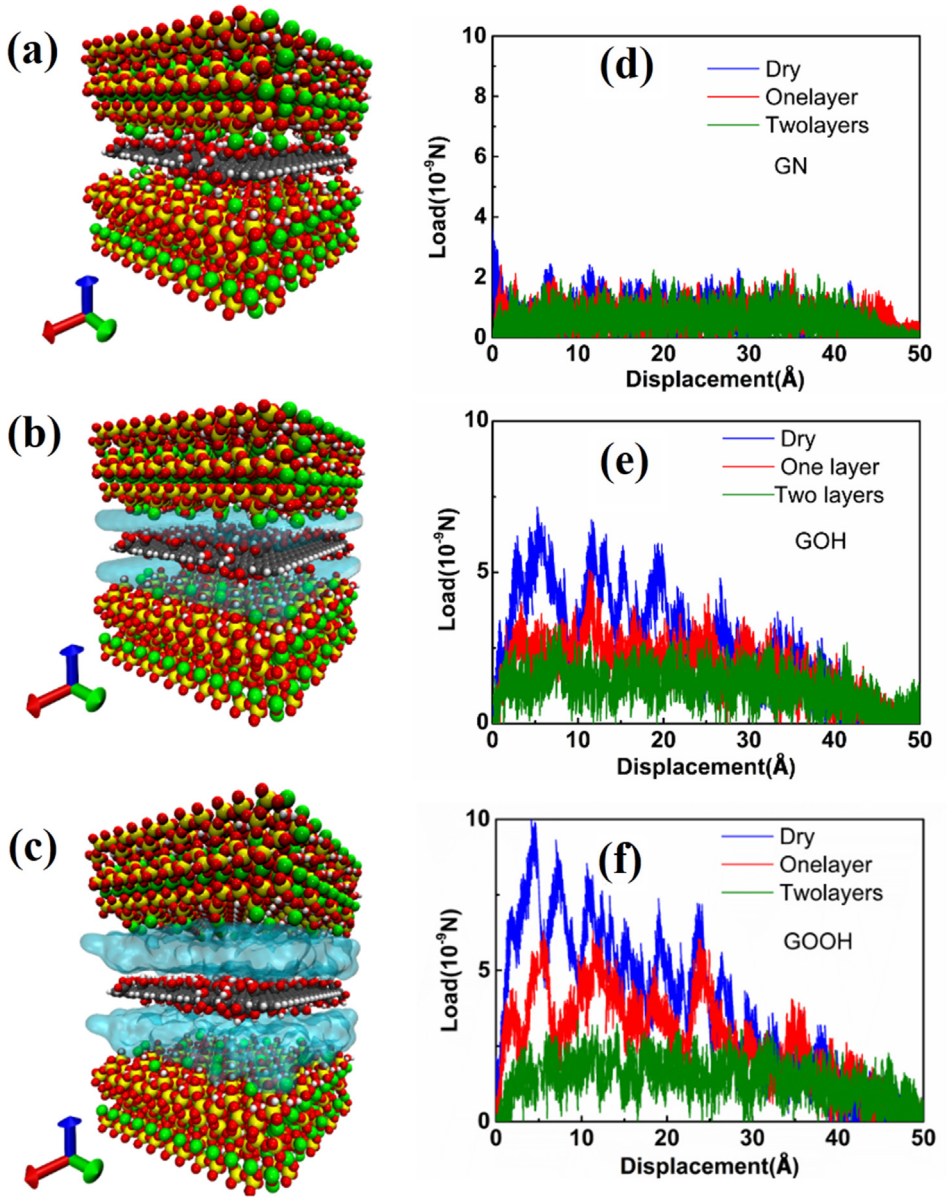

Fig. 9. Initial structure of (a) dry condition model, (b) one-layer water molecular model, and (c) two-layers water molecular model. Load-Displacement curves at different water contents for (d) GN, (e) GOH and (f) GOOH, respectively.

CRediT authorship contribution statement

Wang Pan: Data curation, Formal analysis, Investigation, Methodology, Software, Visualization, Writing - original draft. **Qiao Gang:** Data curation, Formal analysis, Software. **Guo Yupeng:** Writing - original draft, Writing - review & editing. **Zhang Yue:** Methodology. **Hou Dongshuai:** Conceptualization, Funding acquisition, Investigation, Project administration, Resources, Supervision, Validation. **Jin Zuquan:** Writing - review & editing. **Zhang Jinrui:** Funding acquisition, Project administration, Resources, Supervision, Validation. **Wang Muhan:** Visualization. **Hu Xiaoxia:** Writing - review & editing.

Declaration of Competing Interest

The authors declare that they have no known competing financial interests or personal relationships that could have appeared to influence the work reported in this paper.

Acknowledgement

Financial support from National Natural science foundation of China under Grant U1806225, 51908308, 51978352, Natural science foundation of Shandong Province under Grant ZR2019PEE004, China Postdoctoral Science Foundation under Grant 2019M652345, and State Key Laboratory of High Performance Civil Engineering Materials under Grant 2018CEM012.

References

[1] S. Chakraborty, S.P. Kundu, A. Roy, B. Adhikari, S.B. Majumder, Effect of jute as fiber reinforcement controlling the hydration characteristics of cement matrix, Indus. Eng. Chem. Res. 52 (3) (2013) 1252–1260.
[2] T. Zhang, P. Gao, P. Gao, J. Wei, Q. Yu, Effectiveness of novel and traditional methods to incorporate industrial wastes in cementitious materials—An overview, Resources, Conservation Recycling 74 (2013) 134-143.
[3] R.V. Sagar, B.R. Prasad, S.S. Kumar, An experimental study on cracking evolution in concrete and cement mortar by the b-value analysis of acoustic emission technique, Cem. Concr. Res. 42 (8) (2012) 1094–1104.

[4] K.Y. Kim, T.S. Yun, K.P. Park, Evaluation of pore structures and cracking in cement paste exposed to elevated temperatures by X-ray computed tomography, Cem. Concr. Res. 50 (2013) 34–40.
[5] K. Van Tittelboom, N. De Belie, F. Lehmann, C.U. Grosse, Acoustic emission analysis for the quantification of autonomous crack healing in concrete, Constr. Build. Mater. 28 (1) (2012) 333–341.
[6] P.S. Song, S. Hwang, Mechanical properties of high-strength steel fiber-reinforced concrete, Constr. Build. Mater. 18 (9) (2004) 669–673.
[7] M. Ali, A. Liu, H. Sou, N. Chouw, Mechanical and dynamic properties of coconut fibre reinforced concrete, Constr. Build. Mater. 30 (2012) 814–825.
[8] J. Reis, Fracture and flexural characterization of natural fiber-reinforced polymer concrete, Constr. Build. Mater. 20 (9) (2006) 673–678.
[9] P. Soroushian, J.-P. Won, M. Hassan, Durability characteristics of CO2-cured cellulose fiber reinforced cement composites, Constr. Build. Mater. 34 (2012) 44–53.
[10] H. Su, J. Xu, Dynamic compressive behavior of ceramic fiber reinforced concrete under impact load, Constr. Build. Mater. 45 (2013) 306–313.
[11] N. Morova, Investigation of usability of basalt fibers in hot mix asphalt concrete, Constr. Build. Mater. 47 (2013) 175–180.
[12] S. Chuah, Z. Pan, J.G. Sanjayan, C.M. Wang, W.H. Duan, Nano reinforced cement and concrete composites and new perspective from graphene oxide, Constr. Build. Mater. 73 (2014) 113–124.
[13] L.P. Singh, S.R. Karade, S.K. Bhattacharyya, M.M. Yousuf, S. Ahalawat, Beneficial role of nanosilica in cement based materials - A review, Constr. Build. Mater. 47 (2013) 1069–1077.
[14] M. Saafi, Wireless and embedded carbon nanotube networks for damage detection in concrete structures, Nanotechnology 20 (39) (2009).
[15] S. Chuah, Z. Pan, J.G. Sanjayan, C.M. Wang, W.H. Duan, Nano reinforced cement and concrete composites and new perspective from graphene oxide, Constr. Build. Mater. 73 (2014) 113–124.
[16] K.S. Novoselov, A.K. Geim, S.V. Morozov, D. Jiang, Y. Zhang, S.V. Dubonos, I.V. Grigorieva, A.A. Firsov, Electric field effect in atomically thin carbon films, Sci. 306 (5696) (2004) 666–669.
[17] I. Ahmad, M. Islam, H.S. Abdo, T. Subhani, K.A. Khalil, A.A. Almajid, B. Yazdani, Y. Zhu, Toughening mechanisms and mechanical properties of graphene nanosheet-reinforced alumina, Mater. Des. 88 (2015) 1234–1243.
[18] Y. Pan, T. Wu, H. Bao, L. Li, Green fabrication of chitosan films reinforced with parallel aligned graphene oxide, Carbohydr. Polym. 83 (4) (2011) 1908–1915.
[19] T. Ramanathan, A. Abdala, S. Stankovich, D. Dikin, M. Herrera-Alonso, R. Piner, D. Adamson, H. Schniepp, X. Chen, R. Ruoff, Functionalized graphene sheets for polymer nanocomposites, Nat. Nanotechnol. 3 (6) (2008) 327.
[20] X. Huang, Z. Yin, S. Wu, X. Qi, Q. He, Q. Zhang, Q. Yan, F. Boey, H. Zhang, Graphene-based materials: synthesis, characterization, properties, and applications, Small 7 (14) (2011) 1876–1902.
[21] K. Xia, H. Zhan, D.a. Hu, Y. Gu, Failure mechanism of monolayer graphene under hypervelocity impact of spherical projectile, Sci. Rep. 6 (2016) 33139.
[22] R.S. Edwards, K.S. Coleman, Graphene synthesis: relationship to applications, Nanoscale 5 (1) (2013) 38–51.
[23] V.C. Tung, M.J. Allen, Y. Yang, R.B. Kaner, High-throughput solution processing of large-scale graphene, Nat. Nanotechnol. 4 (1) (2009) 25.
[24] H. Zhan, G. Zhang, J.M. Bell, Y. Gu, Graphene with patterned fluorination: morphology modulation and implications, J. Phys. Chem. C 119 (49) (2015) 27562–27568.
[25] M. Saafi, L. Tang, J. Fung, M. Rahman, J. Liggat, Enhanced properties of graphene/fly ash geopolymeric composite cement, Cem. Concr. Res. 67 (2015) 292–299.
[26] L. Qiu, X. Yang, X. Gou, W. Yang, Z.F. Ma, G.G. Wallace, D. Li, Dispersing carbon nanotubes with graphene oxide in water and synergistic effects between graphene derivatives, Chem.–European J. 16 (35) (2010) 10653–10658.
[27] J.I. Paredes, S. Villar-Rodil, A. Martinez-Alonso, J.M.D. Tascon, Graphene oxide dispersions in organic solvents, Langmuir 24 (19) (2008) 10560–10564.
[28] K. Xu, B. Feng, C. Zhou, A.S. Huang, Synthesis of highly stable graphene oxide membranes on polydopamine functionalized supports for seawater desalination, Chem. Eng. Sci. 146 (2016) 159–165.
[29] K. Gong, Z. Pan, A.H. Korayem, L. Qiu, D. Li, F. Collins, C.M. Wang, W.H. Duan, Reinforcing effects of graphene oxide on portland cement paste, J. Mater. Civ. Eng. 27 (2) (2014) A4014010.
[30] Z. Pan, L. He, L. Qiu, A.H. Korayem, G. Li, J.W. Zhu, F. Collins, D. Li, W.H. Duan, M. C. Wang, Mechanical properties and microstructure of a graphene oxide–cement composite, Cem. Concr. Comp. 58 (2015) 140–147.
[31] D. Hou, Y. Zhu, Y. Lu, Z. Li, Mechanical properties of calcium silicate hydrate (C–S–H) at nano-scale: a molecular dynamics study, Mater. Chem. Phys. 146 (3) (2014) 503–511.
[32] D. Li, W. Zhao, D. Hou, T. Zhao, Molecular dynamics study on the chemical bound, physical adsorbed and ultra-confined water molecules in the nano-pore of calcium silicate hydrate, Constr. Build. Mater. 151 (2017) 563–574.
[33] P. Wang, Q.G. Zhang, M.H. Wang, B. Yin, D.S. Hou, Y. Zhang, Atomistic insights into cesium chloride solution transport through the ultra-confined calcium-silicate-hydrate channel, PCCP 21 (22) (2019) 11892–11902.
[34] D.S. Hou, Z.Y. Lu, X.Y. Li, H.Y. Ma, Z.J. Li, Reactive molecular dynamics and experimental study of graphene-cement composites: structure, dynamics and reinforcement mechanisms, Carbon 115 (2017) 188–208.
[35] D.S. Hou, T.J. Yang, A reactive molecular dynamics study of graphene oxide sheets in different saturated states: structure, reactivity and mechanical properties, PCCP 20 (16) (2018) 11053–11066.
[36] P. Wang, G. Qiao, Y. Zhang, D. Hou, J. Zhang, M. Wang, X. Wang, X. Hu, Molecular dynamics simulation study on interfacial shear strength between calcium-silicate-hydrate and polymer fibers, Constr. Build. Mater. 257 (2020) 119557.
[37] M.F. Kai, L.W. Zhang, K.M. Liew, Graphene and graphene oxide in calcium silicate hydrates: chemical reactions, mechanical behavior and interfacial sliding, Carbon 146 (2019) 181–193.
[38] T.S. Qureshi, D.K.J.C. Panesar, B. Materials, Impact of graphene oxide and highly reduced graphene oxide on cement based composites, 206 (2019) 71-83.
[39] H. Liang, M. Xu, Y. Bu, B. Chen, Y. Zhang, Y. Fu, X. Xu, J.J.A.S.S. Zhang, Confined interlayer water enhances solid lubrication performances of graphene oxide films with optimized oxygen functional groups, 485 (2019) 64-69.
[40] S. Hajilar, B.J.C.M.S. Shafei, Nano-scale investigation of elastic properties of hydrated cement paste constituents using molecular dynamics simulations, 101 (2015) 216-226.
[41] S.J. Murray, V.J. Subramani, R.P. Selvam, K.D.J.T.R.R. Hall, Molecular dynamics to understand the mechanical behavior of cement paste, 2142(1) (2010) 75-82.
[42] R. Allington, D. Attwood, I. Hamerton, J. Hay, B.J.C.P.A.A.S. Howlin, Manufacturing, A model of the surface of oxidatively treated carbon fibre based on calculations of adsorption interactions with small molecules, 29(9-10) (1998) 1283-1290.
[43] S. Jiao, Z. Xu, Selective gas diffusion in graphene oxides membranes: a molecular dynamics simulations study, ACS Appl. Mater. Interf. 7 (17) (2015) 9052–9059.
[44] R.T. Cygan, J.-J. Liang, A.G. Kalinichev, Molecular models of hydroxide, oxyhydroxide, and clay phases and the development of a general force field, J. Phys. Chem. B 108 (4) (2004) 1255–1266.
[45] P. Dauber-Osguthorpe, V.A. Roberts, D.J. Osguthorpe, J. Wolff, M. Genest, A.T.J. P.S. Hagler, Function,, Bioinformatics, Structure and energetics of ligand binding to proteins: Escherichia coli dihydrofolate reductase-trimethoprim, a drug-receptor system, 4(1) (1988) 31-47.
[46] Y. Wu, H.L. Tepper, G.A.J.T.J.o.c.p. Voth, Flexible simple point-charge water model with improved liquid-state properties, 124(2) (2006) 024503.
[47] M.P. Allen, D.J. Tildesley, Computer simulation of liquids, Oxford university press2017.
[48] F. Sanchez, L.J.J.o.c. Zhang, i. science, Molecular dynamics modeling of the interface between surface functionalized graphitic structures and calcium–silicate–hydrate: interaction energies, structure, and dynamics, 323(2) (2008) 349-358.
[49] F. Sanchez, L.J.C. Zhang, Interaction energies, structure, and dynamics at functionalized graphitic structure–liquid phase interfaces in an aqueous calcium sulfate solution by molecular dynamics simulation, 48(4) (2010) 1210-1223.
[50] J. Yu, Q. Zheng, D. Hou, J. Zhang, S. Li, Z. Jin, P. Wang, B. Yin, X.J.C.P.B.E. Wang, Insights on the capillary transport mechanism in the sustainable cement hydrate impregnated with graphene oxide and epoxy composite, 173 (2019) 106907.
[51] S. Plimpton, P. Crozier, A. Thompson, LAMMPS-large-scale atomic/molecular massively parallel simulator, Sandia National Laboratories 18 (2007) 43.
[52] G.Y. Li, P.M. Wang, X.J.C. Zhao, Mechanical behavior and microstructure of cement composites incorporating surface-treated multi-walled carbon nanotubes, 43(6) (2005) 1239-1245.
[53] D. Fan, L. Lue, S. Yang, Molecular dynamics study of interfacial stress transfer in graphene-oxide cementitious composites, Comput. Mater. Sci. 139 (2017) 56–64.
[54] D. Hou, Z. Li, T.J.R.A. Zhao, Reactive force field simulation on polymerization and hydrolytic reactions in calcium aluminate silicate hydrate (C–A–S–H) gel: structure, dynamics and mechanical properties, 5(1) (2015) 448-461.
[55] W. Li, X. Zheng, B. Liu, X. Sun, T. Wang, J. Zhang, Y. Yan, A novel method for designing carbon nanostructures: tailoring-induced self-scrolling of graphene flakes, Carbon 89 (2015) 272–278.
[56] W. Chen, A.S. Foster, M.J. Alava, L. Laurson, Stick-slip control in nanoscale boundary lubrication by surface wettability, Phys. Rev. Lett. 114 (9) (2015) 095502.